Orbit–orbit interaction and photonic orbital Hall effect in reflection of a light beam*

Zhang Jin(张 进), Zhou Xin-Xing(周新星), Ling Xiao-Hui(凌晓辉), Chen Shi-Zhen(陈世贞), Luo Hai-Lu(罗海陆)†, and Wen Shuang-Chun(文双春)

Key Laboratory for Micro-/Nano-Optoelectronic Devices of Ministry of Education, Hunan University, Changsha 410082, *China*

(Received 24 September 2013; revised manuscript received 11 November 2013; published online 20 April 2014)

We examine the orbit–orbit interaction when a paraxial beam with intrinsic orbital angular momentum (IOAM) reflects at an air–glass interface. The orbital-dependent splitting of the beam intensity distribution arises due to the interaction between IOAM and extrinsic orbital angular momentum (EOAM). In addition, we find that the beam centroid shows an orbital-dependent rotation when seen along the propagation axis. However, the motion of the beam centroid related to the orbit–orbit interaction undergoes a straight line trajectory with a small angle inclining from the propagation axis. Similar to a previously developed spin-dependent splitting in the photonic spin Hall effect, the orbital-dependent splitting could lead to the photonic orbital Hall effect.

Keywords: photonic orbit Hall effect, optical resonance

PACS: 42.25.–p, 41.20.Jb, 42.79.–e **DOI:** 10.1088/1674-1056/23/6/064215

1. Introduction

The orbital angular momentum (OAM) of a light beam can be divided into two parts: intrinsic OAM (IOAM) and extrinsic OAM (EOAM). Here, the IOAM stands for the intrinsic orbital angular momentum associated with OAM around the centroid of the beam, and the EOAM is the extrinsic orbital angular momentum related to the motion of the centroid.[1] The beam with a helical phase front apertured symmetrically about the propagation axis has zero transverse momentum and, consequently, an OAM of $l\hbar$ per photon is independent of the calculation axis.[2] The OAM of the light beam may therefore be described as intrinsic. However, when the beam passes through an off-axis aperture, its transverse momentum is nonzero and the OAM depends upon the choice of calculation axis, and therefore must be described as extrinsic.[3]

Unlike the OAM, the spin angular momentum (SAM) does not depend upon the choice of the calculation axis and is always intrinsic.[4] Recently, the spin–orbit interaction related to spin photons has received considerable attention.[5–12] The photonic spin Hall effect (SHE) is generally believed to be a result of an effective spin–orbit interaction, which describes the mutual influence of the spin (polarization) and the trajectory of the beam centroid related to EOAM.[13–15] The photonic SHE manifests itself as spin-dependent splitting in the beam reflection, refraction on a sharp boundary,[16–23] or propagation in an inhomogeneous medium.[24–27]

In this paper, similar to the previously developed spin–orbit interaction and the photonic SHE on a sharp boundary, we evolve the orbit–orbit (IOAM and EOAM) interaction of light beam reflection at an air–glass interface. The manifestation of the orbit–orbit interaction is the influence of the IOAM on the trajectory of the beam centroid related to the EOAM. To obtain a clear physical picture of the orbit–orbit interaction, we consider the beam reflection near the Brewster angle. We find that the beam centroid shows an orbital-dependent rotation around the propagation axis. However, we show that the motion of the centroid related to the orbit–orbit interaction undergoes a straight line trajectory with a small angle inclining from the propagation axis. In general, a Hermite–Gaussian beam can be represented as a superposition of two Laguerre–Gaussian components with opposite IOAM states.[2] As a result, the orbital-dependent splitting of the beam intensity distribution arises, leading to the photonic orbital Hall effect (OHE).

2. Orbit–orbit interaction

To reveal the orbit–orbit interaction, we first establish a general propagation model to describe IOAM and EOAM. Figure 1 illustrates the Cartesian coordinate system. The z axis of the laboratory Cartesian frame x, y, z is normal to the air–glass interface. In addition, two coordinate systems ($x_{\rm i}$, $y_{\rm i}$, $z_{\rm i}$) and ($x_{\rm r}$, $y_{\rm r}$, $z_{\rm r}$) are introduced to denote the incident beam and the reflection beam, respectively. In the momentum space, the angular spectrum of the incident beam can be written as[2]

$$\tilde{\boldsymbol{E}}_{\rm i} = \left[\alpha\hat{\boldsymbol{x}}_{\rm i} + \beta\hat{\boldsymbol{y}}_{\rm i} - \frac{\alpha k_{x{\rm i}} + \beta k_{y{\rm i}}}{k}\hat{\boldsymbol{z}}_{\rm i}\right]\tilde{u}_{\rm i}, \tag{1}$$

*Project supported by the National Natural Science Foundation of China (Grant Nos. 61025024 and 11074068) and the Innovation Foundation for Postgraduates of Hunan Province, China (Grant No. CX2013B130).

†Corresponding author. E-mail: hailuluo@hnu.edu.cn

© 2014 Chinese Physical Society and IOP Publishing Ltd

and

$$\tilde{u}_{\rm i} = \frac{C_l w_0}{2}\exp\left[-\frac{w_0^2(k_{x\rm i}^2+k_{y\rm i}^2)}{4}\right] \times\left[\frac{w_0\left(-{\rm i}k_{x\rm i}+{\rm sign}[l]k_{y\rm i}\right)}{\sqrt{2}}\right]^{|l|}. \quad (2)$$

Here, α and β are Jones vectors, $\hat{\boldsymbol{x}}_{\rm i}$, $\hat{\boldsymbol{y}}_{\rm i}$, $\hat{\boldsymbol{z}}_{\rm i}$ are unit vectors, and $k=2\pi/\lambda$ is the wave number in a vacuum. The incident angular spectrum is given by $\tilde{u}_{\rm i}$, where w_0 is the radial of the beam waist, and l is the topological charge, $C_l=\sqrt{2/(\pi|l|!)}$ is the normalization constant, and sign$[l]$ is the sign function.

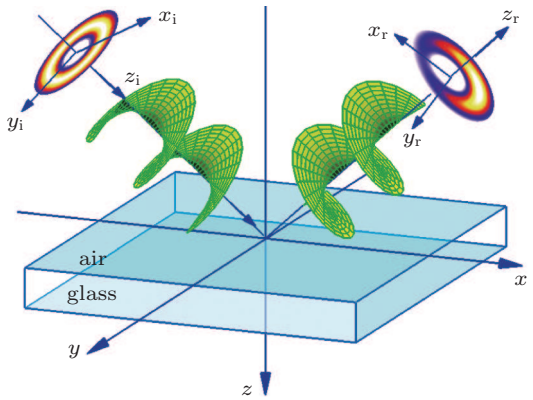


Fig. 1. (color online) Schematic illustrating the paraxial beam with the IOAM reflected at an air–glass interface.

The reflected angular spectrum is related to the incident angular spectrum by means of the relation:[14] $\tilde{\boldsymbol{E}}_{\rm r}=M\tilde{\boldsymbol{E}}_{\rm i}$, and

$$M=\begin{bmatrix} r_{\rm p} & \dfrac{(r_{\rm p}+r_{\rm s})\cot\theta_{\rm i}k_{y\rm r}}{k} & \dfrac{r_{\rm p}k_{x\rm r}}{k} \\ -\dfrac{(r_{\rm p}+r_{\rm s})\cot\theta_{\rm i}k_{y\rm r}}{k} & r_{\rm s} & -\dfrac{r_{\rm s}k_{y\rm r}}{k} \\ -\dfrac{r_{\rm p}k_{x\rm r}}{k} & \dfrac{r_{\rm s}k_{y\rm r}}{k} & 0 \end{bmatrix}. \quad (3)$$

Here, $\theta_{\rm i}$ is the incidence angle, and $r_{\rm p}$ and $r_{\rm s}$ are the Fresnel reflection coefficients for parallel and perpendicular polarizations, respectively. For the arbitrary angular spectrum component, $r_{\rm p}$ and $r_{\rm s}$ can be expanded by making use of the first-order Taylor series expansion

$$r_{\rm p,s}(k_{x\rm i})=r_{\rm p,s}(k_{x\rm i}=0)\left[1+\frac{k_{x\rm i}}{k}\frac{\partial\ln r_{\rm p,s}(k_{x\rm i})}{\partial\theta_{\rm i}}\right]. \quad (4)$$

From Eqs. (1)–(4), we can obtain the reflected angular spectrum as

$$\begin{aligned}\tilde{\boldsymbol{E}}_{\rm r} =& \left[\alpha\left(r_{\rm p}-\frac{\partial r_{\rm p}}{\partial\theta_{\rm i}}\frac{k_{x\rm r}}{k}\right)+\beta\left(r_{\rm s}+r_{\rm p}\right)\cot\theta_{\rm i}\frac{k_{y\rm r}}{k}\right]\tilde{u}_{\rm r}\hat{\boldsymbol{x}}_{\rm r} \\ &+\left[\beta\left(r_{\rm s}-\frac{\partial r_{\rm s}}{\partial\theta_{\rm i}}\frac{k_{x\rm r}}{k}\right)-\alpha\left(r_{\rm s}+r_{\rm p}\right)\cot\theta_{\rm i}\frac{k_{y\rm r}}{k}\right]\tilde{u}_{\rm r}\hat{\boldsymbol{y}}_{\rm r} \\ &-\left(\alpha r_{\rm p}\frac{k_{x\rm r}}{k}+\beta r_{\rm s}\frac{k_{y\rm r}}{k}\right)\tilde{u}_{\rm r}\hat{\boldsymbol{z}}_{\rm r}, \end{aligned} \quad (5)$$

where $\tilde{u}_{\rm r}$ can be obtained from the incident angular spectrum and the boundary conditions: $k_{x\rm r}=-k_{x\rm i}$ and $k_{y\rm r}=k_{y\rm i}$.

The linear momentum currents can be used to analyze the physical nature of the orbit–orbit interaction. In general, the linear momentum currents can be divided into their orbital and spin parts[28,29]

$$\boldsymbol{p}={\rm Im}[\boldsymbol{E}^*\cdot(\nabla)\boldsymbol{E}]+\frac{1}{2}{\rm Im}[\nabla\times(\boldsymbol{E}^*\times\boldsymbol{E})], \quad (6)$$

where the first term is the orbital momentum currents $\boldsymbol{p}^{\rm o}$, the second term is the spin momentum currents $\boldsymbol{p}^{\rm s}$, and $\boldsymbol{E}$ is the electric field in position space. In momentum space, we can rewrite Eq. (6) as

$$\boldsymbol{P} = |G\tilde{\boldsymbol{E}}|^2\boldsymbol{k}+(k_x\hat{\boldsymbol{y}}-k_y\hat{\boldsymbol{x}})(G^*\tilde{E}_x^*G\tilde{E}_y-G\tilde{E}_xG^*\tilde{E}_y^*). \quad (7)$$

We substitute the propagation operator

$$G=\exp\left[{\rm i}kz-\frac{iz}{2k}\left(k_x^2+k_y^2\right)\right]$$

into Eq. (7), and derive the orbital and spin momentums as

$$\boldsymbol{P}^{\rm O}=\langle\tilde{\boldsymbol{E}}|\boldsymbol{k}|\tilde{\boldsymbol{E}}\rangle, \quad \boldsymbol{P}^{\rm S}=\langle\tilde{E}_x|k_x|\tilde{E}_y\rangle\hat{\boldsymbol{y}}-\langle\tilde{E}_y|k_y|\tilde{E}_x\rangle\hat{\boldsymbol{x}}. \quad (8)$$

For paraxial beams, the spin part makes no contribution to the linear momentum and $\boldsymbol{P}^{\rm S}=0$.

We have known that the IOAM stands for the intrinsic orbital angular momentum associated with the OAM around the centroid of the beam. In position space, the angular momentum density denotes $\boldsymbol{j}=\boldsymbol{r}\times\boldsymbol{p}$. In momentum space, we replace $\boldsymbol{r}$ by operator ${\rm i}\partial_{\boldsymbol{k}_\perp}+z\hat{\boldsymbol{z}}$ and obtain

$$\begin{aligned}\boldsymbol{J} =& \langle G\tilde{\boldsymbol{E}}|({\rm i}\partial_{\boldsymbol{k}_\perp}+z\hat{\boldsymbol{z}})\times\boldsymbol{k}|G\tilde{\boldsymbol{E}}\rangle \\ &+\left[\langle G\tilde{E}_y|{\rm i}(\partial_{kx}k_x+\partial_{ky}k_y)|G\tilde{E}_x\rangle\right. \\ &\left.-\langle G\tilde{E}_x|{\rm i}(\partial_{kx}k_x+\partial_{ky}k_y)|G\tilde{E}_y\rangle\right]\hat{\boldsymbol{z}}, \end{aligned} \quad (9)$$

where the first term is the IOAM $\boldsymbol{J}^{\rm IO}$, and the second is the SAM $\boldsymbol{J}^{\rm S}$. It is noteworthy that the transverse spin angular momenta are null, which means $J_x^{\rm S}=J_y^{\rm S}=0$. We substitute the propagation operator into Eq. (9) and have

$$\begin{aligned}\boldsymbol{J}^{\rm IO} =& \langle\tilde{\boldsymbol{E}}|{\rm i}k\partial_{ky}|\tilde{\boldsymbol{E}}\rangle\hat{\boldsymbol{x}}+\langle\tilde{\boldsymbol{E}}|-{\rm i}k\partial_{kx}|\tilde{\boldsymbol{E}}\rangle\hat{\boldsymbol{y}} \\ &+\langle\tilde{\boldsymbol{E}}|{\rm i}(k_y\partial_{kx}-k_x\partial_{ky})|\tilde{\boldsymbol{E}}\rangle\hat{\boldsymbol{z}}, \end{aligned} \quad (10)$$

$$\begin{aligned}\boldsymbol{J}^{\rm S} =& \left[\langle\tilde{E}_y|{\rm i}(\partial_{kx}k_x+\partial_{ky}k_y)|\tilde{E}_x\rangle\right. \\ &\left.-\langle\tilde{E}_x|{\rm i}(\partial_{kx}k_x+\partial_{ky}k_y)|\tilde{E}_y\rangle\right]\hat{\boldsymbol{z}}. \end{aligned} \quad (11)$$

Both the IOAM and the SAM do not depend upon the choice of the axis, for which they are said to be intrinsic.

The EOAM is the extrinsic orbital angular momentum related to the motion of the centroid. If the beam centroid is laterally displaced by $\boldsymbol{r}$, the EOAM can be given by

$$\boldsymbol{J}^{\rm EO}=\boldsymbol{r}\times\boldsymbol{P}^{\rm O}. \quad (12)$$

The angular momentum is intrinsic only if $\boldsymbol{J}^{\mathrm{EO}}$ equals zero for all values of $\boldsymbol{r}$. This condition is satisfied only if the transverse momenta P_x^{O} and P_y^{O} are exactly zero. Even though the transverse momentum is nonzero, the IOAM remains $l\hbar$ per photon. However, it does not follow that the OAM of the beam is intrinsic since the result does depend upon the choice of the calculation axis.[3]

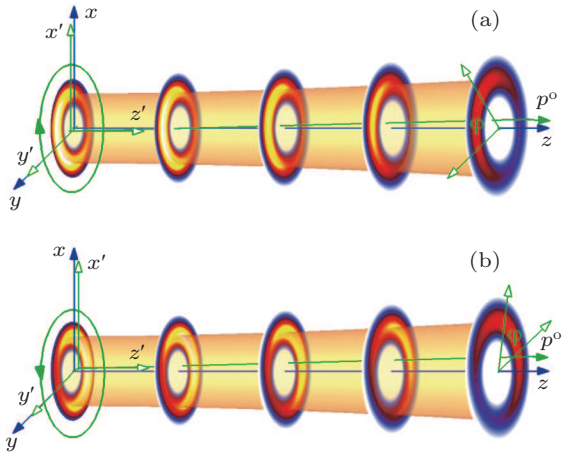


Fig. 2. (color online) The orbital-dependent splitting and rotation effects of beam intensity around the propagation axis in reflection. (a) The beam intensity shows a clockwise rotation for the positive IOAM state $l > 0$. (b) The beam intensity shows an anticlockwise rotation for the negative IOAM state $l < 0$. Here, we choose the incidence angle as $\theta_{\mathrm{i}} = 56°$, the refractive index of glass as $n = 1.515$, the beam waist as $w_0 = 155$ μm, the wave length as $\lambda = 632.8$ nm, and $|l| = 4$. The beam centroid related to the EOAM undergoes a straight line trajectory with a small angle inclining from the propagation axis.

To obtain a clear picture of the orbit–orbit interaction, we reveal how the intensity evolves in reflection. At any given plane $z_{\mathrm{r}} = \mathrm{const}$, the intensity of the reflected beam can be obtained as $I = c^2 p_{z\mathrm{r}}$. Figure 2 shows the orbital-dependent rotation of the beam intensity in different propagation sections. The beam intensity shows a positive transverse shift for the positive IOAM state ($l > 0$), while showing a negative one for the negative IOAM state ($l < 0$). As the propagation distance increases, the intensity distribution shows an orbital-dependent rotation around the propagation axis. For the positive IOAM state, the beam intensity exhibits a clockwise rotation (see Fig. 2(a)). For the negative IOAM state, however, the beam intensity presents an anticlockwise rotation (see Fig. 2(b)). It should be mentioned that these rotation characteristics are observed along the propagation axis. Indeed, the motion of the centroid related to the EOAM undergoes a straight line trajectory with a small angle inclining from the propagation axis. This interesting phenomenon is similar to the beam with IOAM reflection on the glass–air interface near the critical angle.[30]

In general, the orbital-dependent rotation of beam intensity can be explained by the transverse momentum currents as shown in Fig. 3. For the incident beam, the current distribution is symmetric and the transverse momentum is absent (see Figs. 3(a) and 3(e)). For the reflected beam, the current distribution is asymmetric, and therefore produces the transverse momentum. We find that the transverse momentum current presents a clockwise circulation for the positive IOAM state (see Figs. 3(b)–3(d)), while exhibiting an anticlockwise circulation for the negative IOAM state (see Figs. 3(f)–3(h)). Comparing this with Fig. 2, we find that the circulation direction of the momentum currents is the same as that of the beam intensity. As we show below, the asymmetric momentum currents in reflection will lead to the transverse momentum. This interesting phenomenon is similar to the rotation characteristics of an asymmetric beam with both the IOAM and EOAM in free space.[31]

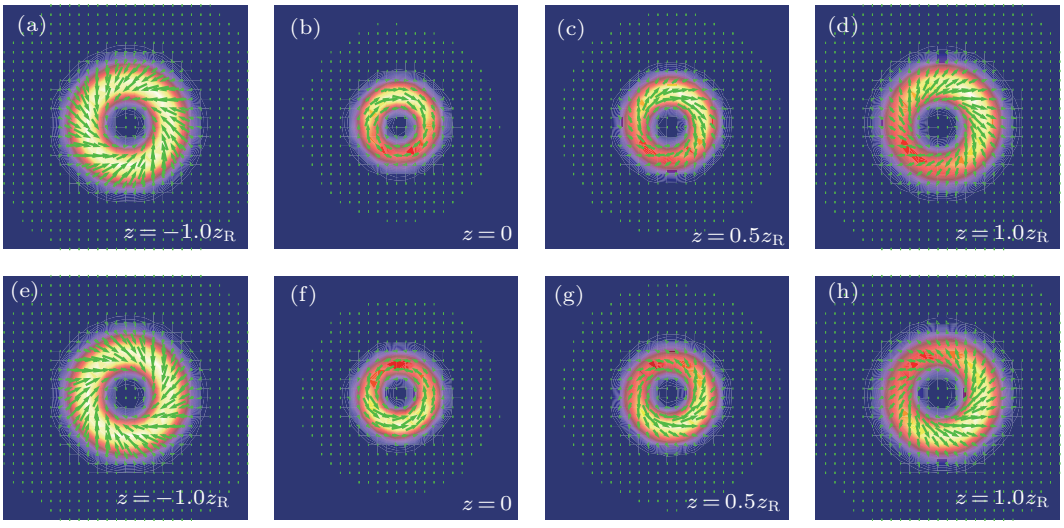


Fig. 3. (color online) Orbital momentum currents of incident and reflected beams. First row: the beam with positive IOAM state. Second row: the beam with negative IOAM state. The background distribution depicts the longitudinal currents, and the green arrows describe the transverse currents. (a) and (e) Cross section of incident beam is chosen as $z_{\mathrm{i}} = -z_{\mathrm{R}}$, where $z_{\mathrm{R}} = k_0 w_0^2/2$ is the Rayleigh length. (b)–(d) and (f)–(h) Reflected beam are plotted in different cross sections. Other parameters are the same as those in Fig. 2 and the intensity is normalized.

3. Photonic orbital Hall effect

We now attempt to reveal the orbital-dependent splitting in momentum space. The centroid of the beam in a given plane $z = \text{const.}$ is given by

$$\langle \boldsymbol{r}_\perp \rangle = \frac{\langle G\tilde{\boldsymbol{E}} | \mathrm{i}\partial_{\boldsymbol{k}_\perp} | G\tilde{\boldsymbol{E}} \rangle}{\langle G\tilde{\boldsymbol{E}} | G\tilde{\boldsymbol{E}} \rangle}, \tag{13}$$

where $\boldsymbol{r}_\perp = x\hat{\boldsymbol{x}} + y\hat{\boldsymbol{y}}$, and $\partial_{\boldsymbol{k}_\perp} = \dfrac{\partial}{\partial k_x}\hat{\boldsymbol{x}} + \dfrac{\partial}{\partial k_y}\hat{\boldsymbol{y}}$. The above equation can be formulated into

$$\langle \boldsymbol{r}_\perp \rangle = \frac{\langle \tilde{\boldsymbol{E}} | \mathrm{i}\partial_{\boldsymbol{k}_\perp} | \tilde{\boldsymbol{E}} \rangle}{\langle \tilde{\boldsymbol{E}} | \tilde{\boldsymbol{E}} \rangle} + \frac{z}{k} \frac{\langle \tilde{\boldsymbol{E}} | \boldsymbol{k}_\perp | \tilde{\boldsymbol{E}} \rangle}{\langle \tilde{\boldsymbol{E}} | \tilde{\boldsymbol{E}} \rangle}. \tag{14}$$

The first and second terms of Eq. (14) are the spatial and angular shifts, which are independent of and dependent on z, respectively.

To enhance the orbital-dependent splitting, we assume that the horizontally polarized beam ($\alpha = 1$, $\beta = 0$) with a helical phase front is incident near the Brewster angle. This is similar to the case that the beam passes through an off-axis aperture,[3] where the orbit–orbit interaction is amplified. To derive the specific expressions of the shifts of the beam centroid, we substitute Eq. (5) into Eq. (14) and obtain

$$\langle x_\mathrm{r} \rangle = -\frac{z(|l|+1)}{kz_\mathrm{R}} \frac{\partial \ln r_\mathrm{p}}{\partial \theta_\mathrm{i}}, \tag{15}$$

$$\langle y_\mathrm{r} \rangle = -\frac{l}{k} \frac{\partial \ln r_\mathrm{p}}{\partial \theta_\mathrm{i}}, \tag{16}$$

where $z_\mathrm{R} = kw_0^2/2$ is the Rayleigh length. This result shows that the transverse shift of the beam centroid is orbital-dependent. It is noteworthy that the present result coincides with previous ones.[32,33] Here, we focus our attention on the case of beam reflection near the Brewster angle. We find that the orbital-dependent shift of the beam centroid will be greatly enhanced, which is similar to the large spin splitting induced by photonic SHE.[34] In addition, the IOAM of a beam can also enhance the geometric SHE when the beam position is observed in a tilted frame of reference.[35] Recently, the strong spin–orbit interaction in metasurface, a two-dimensional electromagnetic nanostructure, enables one to observe a giant photonic SHE.[36,37] Hence, we expect a strong orbit–orbit interaction to arise in the metasurface, and that a giant photonic OHE would occur.

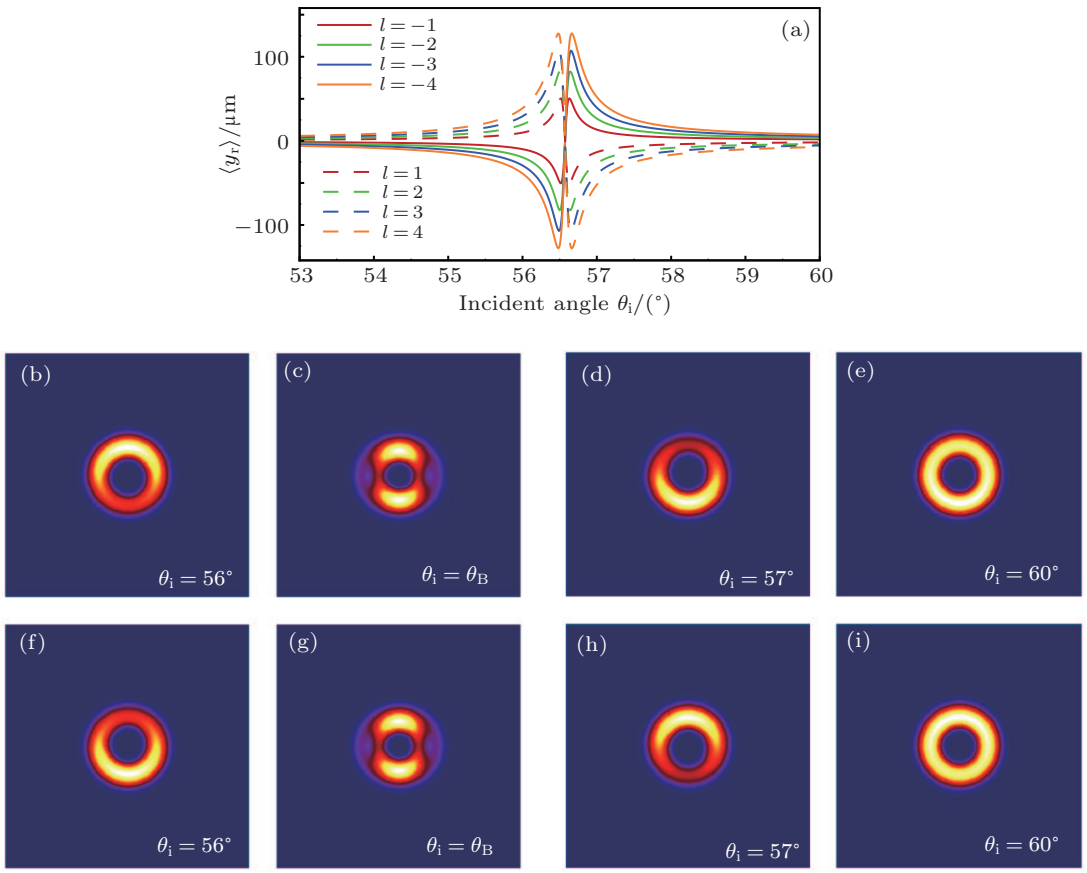


Fig. 4. (color online) Orbital-dependent splitting of beam with opposite IOAM states. (a) Orbital-dependent splitting versus incident angle. (b)–(e) Intensity distribution of a beam with positive IOAM state. (f)–(i) Intensity distribution of a beam with negative IOAM state. The cross section of the beam is chosen as $z_\mathrm{r} = 0$. Other parameters are the same as those in Fig. 2, and the intensity is normalized.

Figure 4 shows the orbital-dependent splitting of the beam centroid in reflection. The theoretical transverse displacements given by Eq. (16) show that the two opposite IOAM states would have opposite tendencies relative to the incident angles (see Fig. 4(a)). This indicates that the orbital-dependent splitting can be greatly enhanced near the Brewster angle (see Figs. 4(b), 4(f), 4(d), and 4(h)). However, the orbital-splitting vanishes when the beam is incident at exactly the Brewster angle (see Figs. 4(c) and 4(g)). When the incident beam is far away from the Brewster angle, the orbital splitting decreases as the incident angle increases, as shown in Figs. 4(e) and 4(i). Indeed, we choose the beam reflection near the Brewster angle to produce an asymmetric intensity distribution.

The angular positions of the beam centroid denote the rotation angle $\tan\varphi = \langle x_r\rangle/\langle y_r\rangle$. Combining Eqs. (15) and (16), the rotation angle is given by

$$\varphi = \arctan\left(\frac{|l|+1}{l}\frac{z_r}{z_R}\right). \tag{17}$$

During the beam propagation from $z_r = 0$ to $z_r = \infty$, the rotation angle amounts to $\pi/2$. The instant angular velocity can be obtained by $\Omega(z) = \mathrm{d}\varphi/\mathrm{d}t = c\,\mathrm{d}\varphi/\mathrm{d}z_r$, so

$$\Omega(z) = c\frac{\dfrac{l}{|l|+1}z_R}{\left(\dfrac{l}{|l|+1}\right)^2 z_R^2 + z_r^2}. \tag{18}$$

We find that the rotation velocity of the beam centroid decreases as the propagation distance increases. When the condition $l = 0$ is satisfied, the rotation characteristics of the beam centroid vanish, i.e., $\Omega(z) = 0$.

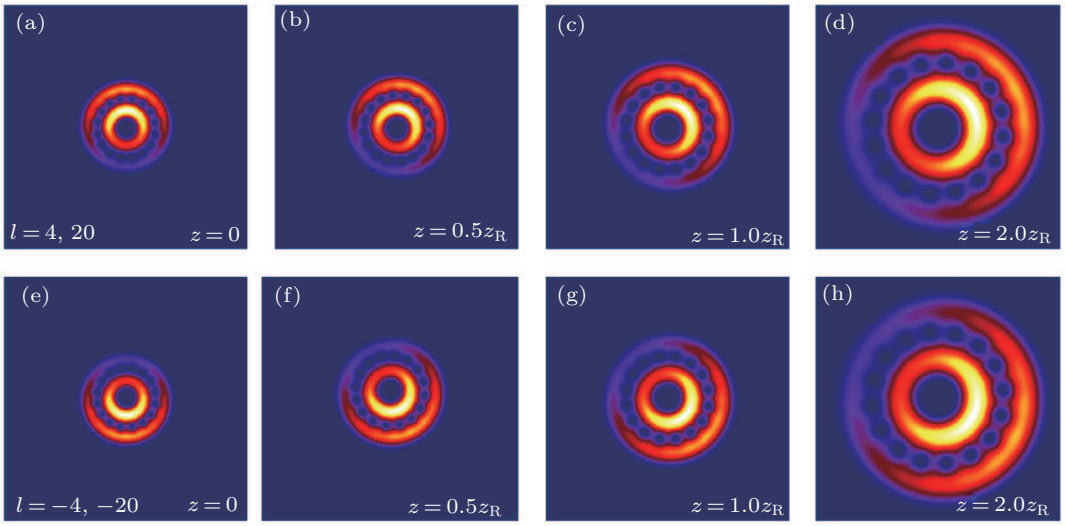


Fig. 5. (color online) Orbital-dependent splitting of the beam with different IOAM states. (a)–(d) Beam with positive IOAM states with $l = 4$ and $l = 20$. (e)–(h) Beam with negative IOAM states with $l = -4$ and $l = -20$. The exterior and inner parts exhibit sightly different rotation velocities. Other parameters are the same as those in Fig. 2 and the intensity is normalized.

Unlike the photonic SHE, which manifests itself as spin-dependent splitting only in two spin states, the photonic OHE shows the orbital-dependent splitting in many IOAM states. Here, we choose the IOAM states $|l| = 4$ and $|l| = 20$ as an example (see Fig. 5). For the positive IOAM states, the beam intensity presents a clockwise rotation (see Figs. 5(a)–5(d)). For the negative IOAM states, however, the beam intensity exhibits an anticlockwise rotation (see Figs. 5(e)–5(h)). In contrast to the photonic SHE counterpart, we emphasize that the photonic OHE can significantly enhance the magnitude of the splitting, since the IOAM states with l can reach even several hundreds. In addition, we also note that the exterior and inner parts of the beam exhibit slightly different rotation velocities, which are exactly given by Eq. (18). It should be noted that the motion of the beam centroid with different IOAM states undergoes different straight line trajectories.

We now perform a quantitative analysis on the linear momenta. Combining Eqs. (1) and (5) with Eq. (8), we obtain the linear momenta of incident and reflected beams as

$$\boldsymbol{P}_i^O = k\hat{\boldsymbol{z}}_i, \tag{19}$$

$$\boldsymbol{P}_r^O = \frac{-(|l|+1)}{z_R} r_p \frac{\partial r_p}{\partial \theta_i}\hat{\boldsymbol{x}}_r + 0\hat{\boldsymbol{y}}_r + k r_p^2 \hat{\boldsymbol{z}}_r. \tag{20}$$

For the incident beam, there is no transverse linear momentum and the OAM is intrinsic. For the reflected beam, however, the transverse linear momentum P_{xr}^O is produced, and the EOAM arises.

The transverse linear momenta are indeed responsible for the angular shifts. For the reflected beam, the shifts of the beam centroid can be expressed as

$$\langle x_r\rangle = \Delta x_r + z_r \Delta\theta_{xr}, \tag{21}$$

$$\langle y_r\rangle = \Delta y_r + z_r \Delta\theta_{yr}. \tag{22}$$

Comparing Eq. (15) with Eq. (16), we find $\Delta x_{\rm r} = 0$ and $\Delta\theta_{\rm yr} = 0$. In the momentum space, we write the angular shifts as

$$\Delta\theta_x = \frac{P_x^{\rm O}}{P_z^{\rm O}}, \quad \Delta\theta_y = \frac{P_y^{\rm O}}{P_z^{\rm O}}. \tag{23}$$

For the incident beam, we have $\Delta\theta_{\rm xi} = 0$ and $\Delta\theta_{\rm yi} = 0$. For the reflected beam, we have

$$\Delta\theta_{\rm xr} = \frac{-(|l|+1)}{kz_{\rm R}} \frac{\partial ln r_{\rm p}}{\partial\theta_{\rm i}}, \quad \Delta\theta_{\rm yr} = 0, \tag{24}$$

which coincides well with Eqs. (15) and (16). These simple results mean that the beam centroid undergoes a straight line trajectory with a small angle inclining from the propagation axis (see Fig. 2).

We now attempt to explore the IOAM and EOAM in reflection. Here, we choose the calculation axis as the propagation axis. Substituting Eq. (5) into Eq. (10) yields

$$\boldsymbol{J}_{\rm r}^{\rm IO} = -lr_{\rm p}\frac{\partial r_{\rm p}}{\partial\theta_{\rm i}}\hat{\boldsymbol{x}}_{\rm r} + 0\hat{\boldsymbol{y}}_{\rm r} - lr_{\rm p}^2\hat{\boldsymbol{z}}_{\rm r}. \tag{25}$$

Substituting Eq. (20) into Eq. (12), we obtain the EOAM as

$$\boldsymbol{J}_{\rm r}^{\rm EO} = -lr_{\rm p}\frac{\partial r_{\rm p}}{\partial\theta_{\rm i}}\hat{\boldsymbol{x}}_{\rm r} + 0\hat{\boldsymbol{y}}_{\rm r} - \frac{l(|l|+1)}{kz_{\rm R}}\left(\frac{\partial r_{\rm p}}{\partial\theta_{\rm i}}\right)^2\hat{\boldsymbol{z}}_{\rm r}. \tag{26}$$

Comparing Eq. (26) with Eq. (25), we find that the transverse angular momentum $\boldsymbol{J}_{\rm xr}^{\rm EO} = \boldsymbol{J}_{\rm xr}^{\rm IO}$ and $\boldsymbol{J}_{\rm yr}^{\rm EO} = \boldsymbol{J}_{\rm yr}^{\rm IO}$. We want to emphasize that these relations are satisfied only if the calculation axis of the EOAM is chosen as the propagation axis.

When the beam centroid exhibits a nonzero transverse angular momentum, we obtain the following relations at the plane of $z_{\rm r} = 0$:

$$\Delta x_{\rm r} = -\frac{J_{\rm yr}^{\rm IO}}{P_{zr}^{\rm O}}, \quad \Delta y_{\rm r} = \frac{J_{\rm xr}^{\rm IO}}{P_{zr}^{\rm O}}. \tag{27}$$

Equation (27) indicates that the spatial shifts have no direct relation with the $z_{\rm r}$-component IOAM $J_{zr}^{\rm IO}$. They are dependent on the transverse angular momentum $\boldsymbol{J}_{\perp}^{\rm IO}$ and the $z_{\rm r}$-component linear momentum $P_{zr}^{\rm O}$.[38] From Eq. (12), we can obtain the following relations:

$$\Delta x_{\rm r} = -\frac{J_{\rm yr}^{\rm EO}}{P_{zr}^{\rm O}}, \quad \Delta y_{\rm r} = \frac{J_{\rm xr}^{\rm EO}}{P_{zr}^{\rm O}}, \tag{28}$$

which depend on the choice of the calculation axis. The EOAM of the beam centroid vanishes if we transfer the calculation axis from xyz to $x'y'z'$ as shown in Fig. 2.

Figure 6 shows the experimental setup to verify the theoretical discussion. A fundamental Gaussian beam generated by a He–Ne laser (Thorlabs HNL210L) passes through the collimating system and a polarizer (GLP1) to produce a horizontal polarized beam. The fundamental Gaussian beam is modulated by a liquid-crystal spatial light modulator (Holoeye Pluto) to obtain a vortex beam with IOAM. The beam alters its polarization after the focusing lens, and the GLP2 is needed to modulate the incident beam to be horizontally polarized. When the focusing beam with a waist of $w_0 = 155$ μm impinges onto the prism interface, the EOAM is produced due to the orbit–orbit interaction. As a result of the orbit–orbit interaction, the opposite shifts of the two orbital components show dependence on the input IOAM state. The prism is mounted to a rotation stage, which allows precise control of the incident angle. The intensity distribution profiles can be detected by a CCD (Coherent LaserCam HR) at different propagation distances.

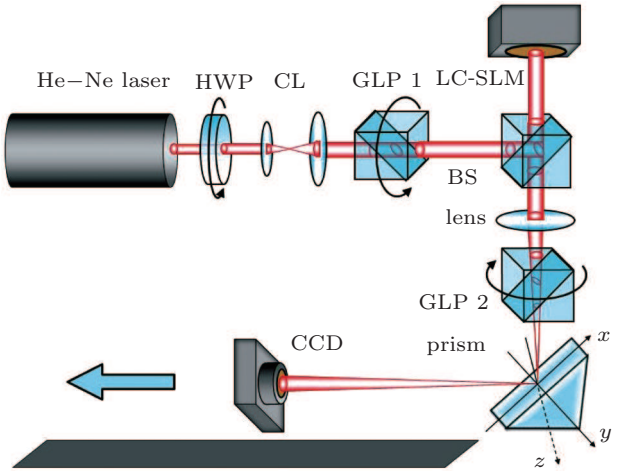


Fig. 6. (color online) Experimental setup for the orbit-dependent rotation effects of the beam centroid. The linearly polarized He–Ne laser source (21 mW and 632.8 nm); HWP denotes the half-wave plate (for adjusting the intensity); CL denotes the collimating lenses with focal lengths of 25 mm and 125 mm, respectively; GLP1 and GLP2 denotes the Glan laser polarizers; LC-SLM denotes the liquid crystal spatial light modulator; BS: non-polarizing beam splitter; lenses have an effective focal length of 750 mm; prism has a refractive index $n = 1.515$; and CCD denotes the charge-coupled device.

Figure 7 shows the theoretical and experimental results of orbit-dependent splitting and intensity rotation of beam after reflection at the air–glass interface. To obtain a clear picture of orbit-dependent splitting, we choose the IOAM states as $|l| = 4$. From Fig. 7 we find that the orbit-dependent splitting of the beam intensity arises. The beam centroid present a positive transverse shift for the positive IOAM state, while a negative one for the negative IOAM state. As the propagation distance increases, the intensity distribution presents an orbit-dependent rotation around the propagation axis. For the positive IOAM state, the beam centroid presents a clockwise rotation (see Figs. 7(a)–7(d)). For the negative IOAM state, however, the beam centroid exhibits an anticlockwise rotation (see Figs. 7(e)–7(h)). Figures 7(a′)–7(d′) and 7(e′)–7(h′) show the experimental results which agree well with the theoretical prediction. Note that the Hermite–Gaussian beams can be represented as a superposition of two Laguerre–Gaussian components with opposite IOAM states.[2] As a result, the orbit-dependent splitting of the beam intensity distribution arises. Thus, the orbit–orbit interaction would lead to the photonic OHE.

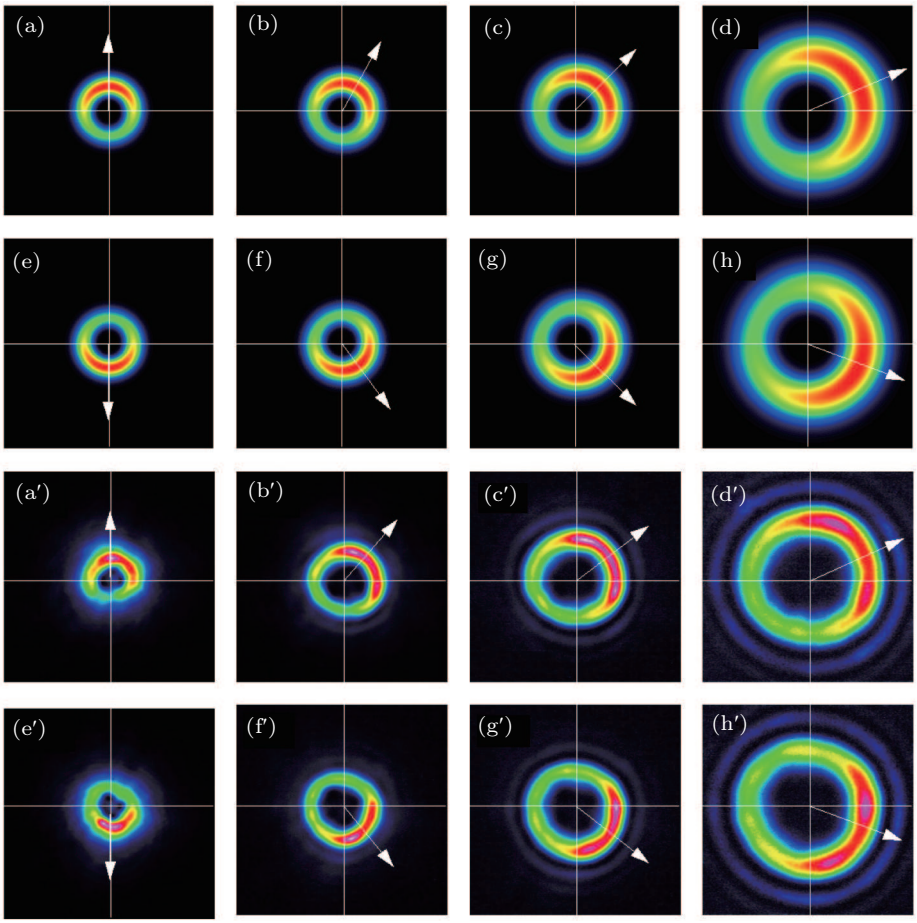


Fig. 7. (color online) Theoretical and experimental results of the orbit-dependent splitting and intensity rotation. (a)–(d) Theoretical results of the beam with positive IOAM state. (e)–(h) Theoretical results of the beam with negative IOAM states. (a′)–(d′) Experimental results of the beam with positive IOAM states. (e′)–(h′) Experimental results of the beam with negative IOAM states. Other parameters are the same as those in Fig. 2 and the intensity is normalized.

4. Conclusions

In this paper, we have examined the orbit–orbit interaction when a paraxial beam with intrinsic orbital angular momentum (IOAM) reflects at an air–glass interface. Similar to the spin–orbit interaction in the photonic spin Hall effect (SHE), we have dealt with the issue of how the extrinsic orbital angular momentum (EOAM) arises and the orbit–orbit interaction presents. We have obtained a large orbit-dependent splitting near the Brewster angle, which provides clear evidence for the photonic orbital Hall effect (OHE). The orbit-dependent splitting can be directly detected without the need of the signal enhancement technique known as weak measurements. The photonic SHE has been regarded as a direct optical analogy of the SHE in an electronic system. Recently, important progress has been made in electronic beams with IOAM.[39–42] Due to the close similarity between photonic and electronic beams, we predict that the photonic OHE can also be extended to electronic systems and the exploration of electronic OHE would probably provide many interesting insights into the orbit–orbit interaction.

References

[1] Bliokh K Y 2006 *Phys. Rev. Lett.* **97** 043901
[2] Allen L, Beijersbergen M W, Spreeuw R J C and Woerdman J P 1992 *Phys. Rev. A* **45** 8185
[3] O'Neil A T, MacVicar I, Allen L and Padgett M J 2002 *Phys. Rev. Lett.* **88** 053601
[4] Beth R A 1936 *Phys. Rev.* **50** 115
[5] Liberman V S and Zeldovich B Y 1992 *Phys. Rev. A* **46** 5199
[6] Marrucci L, Manzo C and Paparo D 2006 *Phys. Rev. Lett.* **96** 163905
[7] Zhao Y, Edgar J S, Jeffries G D M, McGloin D and Chiu D T 2007 *Phys. Rev. Lett.* **99** 073901
[8] Bliokh K Y, Niv A, Kleiner V and Hasman E 2008 *Nat. Photon.* **2** 748
[9] Haefner D, Sukhov S and Dogariu A 2009 *Phys. Rev. Lett.* **102** 123903
[10] Rodríguez-Herrera O G, Lara D, Bliokh K Y, Ostrovskaya E A and Dainty C 2010 *Phys. Rev. Lett.* **104** 253601
[11] Vuong L T, Adam A J L, Brok J M, Planken P C M and Urbach H P 2010 *Phys. Rev. Lett.* **104** 083903
[12] Shitrit N, Yulevich I, Maguid E, Ozeri D, Veksler D, Kleiner V and Hasman E 2013 *Science* **340** 724
[13] Onoda M, Murakami S and Nagaosa N 2004 *Phys. Rev. Lett.* **93** 083901
[14] Bliokh K Y and Bliokh Y P 2006 *Phys. Rev. Lett.* **96** 073903
[15] Hosten O and Kwiat P 2008 *Science* **319** 787
[16] Bliokh K Y and Bliokh Y P 2007 *Phys. Rev. E* **75** 066609
[17] Aiello A and Woerdman J P 2008 *Opt. Lett.* **33** 1437
[18] Qin Y, Li Y, He H and Gong Q H 2009 *Opt. Lett.* **34** 2551
[19] Ménard J M, Mattacchione A E, van Driel H M, Hautmann C and Betz M 2010 *Phys. Rev. B* **82** 045303
[20] Luo H L, Zhou X X, Shu W X, Wen S C and Fan D Y 2011 *Phys. Rev. A* **84** 043806

[21] Kong L J, Wang X L, Li S M, Li Y N, Chen J, Gu B and Wang H T 2012 *Appl. Phys. Lett.* **100** 071109
[22] Tang M, Zhou X X, Luo H L and Wen S C 2012 *Chin. Phys. B* **21** 124201
[23] Pan M M, Li Y, Ren J L, Wang B, Xiao Y F, Yang H and Gong Q H 2013 *Appl. Phys. Lett.* **103** 071106
[24] Gorodetski Y, Niv A, Kleiner V and Hasman E 2008 *Phys. Rev. Lett.* **101** 043903
[25] Shitrit N, Bretner I, Gorodetski Y, Kleiner V and Hasman E 2011 *Nano Lett.* **11** 2038
[26] Kang M, Chen J, Gu B, Li Y, Vuong L T and Wang H T 2012 *Phys. Rev. A* **85** 035801
[27] Ling X H, Zhou X X, Luo H L and Wen S C 2012 *Phys. Rev. A* **86** 053824
[28] Bekshaev A Y and Soskin M S 2007 *Opt. Commun.* **271** 332
[29] Berry M V 2009 *J. Opt. A: Pure Appl. Opt.* **11** 094001
[30] Okuda H and Sasada H 2008 *J. Opt. Soc. Am. A* **25** 881
[31] Luo H L, Wen S C, Shu W X and Fan D Y 2010 *Phys. Rev. A* **81** 053826
[32] Bliokh K Y, Shadrivov I V and Kivshar Y S 2009 *Opt. Lett.* **34** 389
[33] Merano M, Hermosa N, Woerdman J P and Aiello A 2010 *Phys. Rev. A* **82** 023817
[34] Zhou X X, Luo H L and Wen S C 2012 *Opt. Express* **20** 16003
[35] Kong L J, Qian S X, Ren Z C, Wang X L and Wang H T 2012 *Phys. Rev. A* **85** 035804
[36] Yin X B, Ye Z L, Rho J, Wang Y and Zhang X 2013 *Science* **339** 1405
[37] Li G X, Kang M, Chen S M, Zhang S, Pun E Y B, Cheah K W and Li J 2013 *Nano Lett.* **13** 4148
[38] Aiello A, Lindlein N, Marquardt C and Leuchs G 2009 *Phys. Rev. Lett.* **103** 100401
[39] Bliokh K Y, Bliokh Y P, Savelév S and Nori F 2007 *Phys. Rev. Lett.* **99** 190404
[40] Uchida M and Tonomura A 2010 *Nature* **464** 737
[41] Verbeeck J, Tian H and Schattschneider P 2010 *Nature* **467** 301
[42] McMorran B, Agrawal A, Anderson I, Herzing A, Lezec H, McClelland J and Unguris J 2011 *Science* **331** 192